MULTI-SCALE MODELING OF POLY(3-HEXYLTHIOPHENE) AND [6,6]-PHENYL-C_{61}-BUTYRIC ACID METHYL ESTER USING COARSE GRAINED FORCE FIELD DERIVED FROM DFT BASED ATOMISTIC FORCE FIELD

A Thesis
Presented to
The Academic Faculty

by

Hanjong Yoo

In Partial Fulfillment
of the Requirements for the Degree
Masters in the
School of Materials Science and Engineering

Georgia Institute of Technology
December 2015

MULTI-SCALE MODELING OF POLY(3-HEXYLTHIOPHENE) AND [6,6]-PHENYL-C_{61}-BUTYRIC ACID METHYL ESTER USING COARSE GRAINED FORCE FIELD DERIVED FROM DFT BASED ATOMISTIC FORCE FIELD

Approved by:

Dr. Seung Soon Jang, Advisor
School of Materials Science and Engineering
Georgia Institute of Technology

Dr. John R. Reynolds
School of Materials Science and Engineering
Georgia Institute of Technology

Dr. Paul S. Russo
School of Materials Science and Engineering
Georgia Institute of Technology

Date Approved: Nov. 24th, 2015

ACKNOWLEDGEMENTS

There are many people I want to thank. Without them, the thesis might not be written.

To my advisor, Dr. Seung Soon Jang, I want to thank for the support, suggestions, guidance, and advices that benefited me in the completion of this thesis. Since my undergraduate years, he was always supportive and he always gave me valuable comments so I could go through the hardship.

I also want to thank my parents for the unlimited supports and inspiration to me throughout my life. Because of them, I could make this far and continue my study. Although I am physically thousands miles away from them, I could always feel their love in my heart.

Thanks to my dear girlfriend, Ji Young Shim. I want to thank her especially for her emotional support. When I struggled with researches and studies, she always listened and inspired me.

I wish to thank Dr. Ki Chul Kim for his support on my computational studies. When I asked any kinds of questions, he was always answering my questions and helping me solving problems I faced.

Lastly, I want to thank all graduate students and post docs in the Computational Nanobio Technology lab, especially Ben Chun. They taught me the graduate student's life and the computation skills from the day 1. Without them, I could not make this far.

TABLE OF CONTENTS

LIST OF TABLES

LIST OF FIGURES

SUMMARY

The power conversion efficiencies for the organic photovoltaic cells containing active layers of electron donors and acceptors are dependent of three morphological properties, namely the domain size of the electron donor phase, the interface-to-volume ratio of the blend and the percolation ratio. In this study, poly(3-hexylthiophene) (P3HT), poly(3-nonylthiophene) (P3NT), poly(3-dodecylthiophene) (P3DT), fullerene (C_{60}) and [6,6]-phenyl-C_{61}-butyric acid methyl ester (PCBM) blends have been introduced as the active layers to understand the effect of the structural deformation of the active layer components on the morphological properties. The state-of-the-art coarse grained molecular dynamics simulations are employed to investigate the morphological properties of the active layer systems. We have developed Morse potential-based force field parameters to accurately describe potential energy surfaces between C60 and P3HT coarse grained models. Using the coarse-grained model, we can investigate much larger system during longer simulation time than using full atomistic model. We modified the electron donor and acceptor materials and analyzed how the modifications affect the morphological quantities of active layer in both microscopic macroscopic scales with weight ratio of 1:1.

CHAPTER 1

INTRODUCTION

Solar energy is an environment-friendly energy to replace fossil fuels. Among various devices to transform solar power to electricity, organic photovoltaic cell has a great potential for clean energy production technologies due to its particular properties such as light-weight, mechanical flexibility, and low production cost. [1] Bulk-heterojunction (BHJ) organic photovoltaic cell, a type of device architectures, is considered as state–of-the-art active layer morphology which was first introduced by Yu et al. [2] In BHJ active layer structures, the electron donor materials mostly consist of semiconducting conjugated polymers; on the other hand, the electron acceptor materials employ components with the strong electron affinity such as fullerene derivatives and carbon nanotubes. [3] To date, poly(3-hexylthiophene) (P3HT) and [6,6]-phenyl-C61-butyric acid methyl ester (PCBM) have been recognized as the most popular electron donor-acceptor combination used for the BHJ active layer structures. P3HT is able to transport charge carriers among inter-chains efficiently, and PCBM is much soluble in organic solvents than $C_{60.}$ [4] Also, PCBM has strong electron affinity. [5] The combination of P3HT and PCBM results in relatively high efficiency and stability. [6] Despite their strengths, the organic photovoltaic cells still have hallenges to be resolved for the commercialization. Especially, its low power conversion, whose efficiency is frequently reported to be 12%, [7] is one of the biggest challenges. To improve the power efficiency, the properties of the organic photovoltaic cell system such as device architectures, electron donor-acceptor materials, and active layer morphologies have been studied. Particularly, the morphology of the active layers has been known to be a critical factor determining the performance. For instance, Mazzio *et al.* suggested that the excitons generated by the incident solar light would generate the electron and hole pair.

The exciton diffuses into the electron donor and acceptor interface and separated into electrons and holes. Then, electrons that are absorbed by the acceptor and the holes that are accepted by the donor are transported to each electrode. [1] From the working mechanism of the organic photovoltaics, the exciton dissociation is critical to the efficiency of the organic photovoltaics and the bulk-heterojunction, the state of the art device architecture, offers the largest donor and acceptor interface comparing to the both single layer and bilayer architectures. Therefore, the morphology of the active layer is closely related to the cell efficiency.

To date, a series of researches have been extensively launched to study the correlation of the morphology of the active layers with the cell performance, and thereby figure out the optimal morphology for the most efficient performance of the organic photovoltaic cells. Swinnen et al. [8] investigated the effect of thermal annealing on the morphology of the active layer. They employed a various annealing processes and observed the large sized P3HT crystallites at low annealing temperature (75-115°C) for a short time (5 min). However, in the case of either longer annealing process or higher temperature annealing (120-150°C), the size of PCBM crystallites grew and formed needle-like structures that hinder the overall efficiency of the devices. Ma et al. replaced chloroform with chlorobenzene as solvent. Chlorobenzene prevented massive growth of PCBM aggregates and it aided to optimize the morphology of the active layer for the stable phase separation. Despite these experimental efforts, it is still hard to analyze the morphology of the active layers in molecular levels and thereby it is limited to correlate the cell performance with the active layer morphology such as the interface-to-volume ratios and the percolation ratios. [5]

Recently, the state of the art molecular dynamics (MD) methodology has been utilized for better understanding on the active layer morphology in molecular levels. To and Adams implemented the MD simulations using the coarse grained model. With the coarse grained model, they investigated PCBM-P3HT interfaces for the different

crystalline orientation, and amorphous P3HT. To observe the crystallinity of either P3HT or PCBM in the system, they implemented the orientational order parameter. More crystalline P3HT was observed near the interface of face-on orientation that the side of thiophene is faced PCBM and amorphous structure. On the other hand, end-on and edge-on orientation that the side of P3HT parallel each other in Y and Z direction, respectively, did not show such a trend due to weaker interfacial energy. [9] Lee et al. [5] studied the morphology of P3HT:PCBM blends via the MD simulations. They analyzed the morphological properties such as interface to volume ratio for the exciton dissociation, domain size for the exciton diffusion and percolation ratio of both the donor and acceptor regions using spatial-discretization method while varying weight ratios of PCBM and P3HT. Through the analysis, they observed that the weight ratio of 1:1 in PCBM-P3HT blend was the optimum ratio that exhibits the largest interface-to-volume ratio and the balanced percolation ratio between PCBM and P3HT.

In this work, we followed the coarse-graining approach of To and Adams but developed completely different force field parameters using Morse potential functions that allowed us to adjust the energy surface moderately realistic To and Adams measured the melting temperature to validate their force field. They assumed the melting temperature based on the discontinuities in the density versus the temperature curve. [9] However, it is very dangerous assumption because it is hard to insist whether the system is melted at the certain point in the molecular dynamics simulation. In our work, we not only optimized (modified) to describe both intermolecular and intramolecular interactions in simulations but also validate our force field with two experimental data, the density and the solubility parameter of each component. In addition, Lee et al. [5] developed coarse-grained force field where the PCBM molecule was coarse grained into a single pseudo atom and each P3HT repeat unit was coarse grained into a single bead. Due to this extreme simplification, the obvious drawback was the huge loss of accuracy in the calculation. However, they investigated the morphological properties of the active layer

from different angle. Therefore, we followed their approach with coarse grain force field to determine the morphological properties that is strongly related to the efficiency of the organic photovoltaics. We developed various combinations of electron donor and acceptor materials. Then, the state of the art coarse-grained MD simulations were employed to quantify and analyze the morphological properties such as the pair correlation function, the coordination number, and interface to volume ratio affecting the performance of the organic photovoltaic cells.

CHAPTER 2

MODELING AND SIMULATION

FORCE FIELD DEVELOPMENT AND SIMULATION PARAMETERS

Atomistic models with force field parameters were prepared as reference models. We therefore adopted the DREIDING force field parameters [10] for the intermolecular interactions in the atomistic models of P3HT-P3HT and PCBM-PCBM pairs. The DREIDING force field is shown below.

$$E_{total} = E_{vdW} + E_{Q} + E_{bond} + E_{angle} + E_{torsion} + E_{inversion} \quad (1)$$

where E_{total}, E_{vdW}, E_{Q}, E_{bond}, E_{angle}, $E_{torsion}$, $E_{inversion}$ are the total, van der Waals, electrostatic, bond stretching, angle bending, torsion, and inversion energy functions, respectively. The DREIDING force field is a generic force field for nonmetallic main group elements such as carbon, nitrogen, oxygen, hydrogen and a few metals.[11] On the other hand, the DREIDING force field based intermolecular interactions in the thiophene-fullerene pair had never been validated, and thereby the force field for this pair was newly developed in the course of the simulation. To obtain the potential energy surface of the intermolecular interactions vigorously, the density functional theory (DFT) calculations were employed. Geometry optimizations were performed using Jaguar 7.6 with the General Gradient Approximation (GGA) Perdew-Burke-Ernzerhof (PBE) functional. The DFT-D3 correction[12] was used with PBE functional to control dispersion interaction.[13] The atomic charges were assigned through Mulliken population method using PBE-D3 and 6-31G**.

MODEL CONSTRUCTION

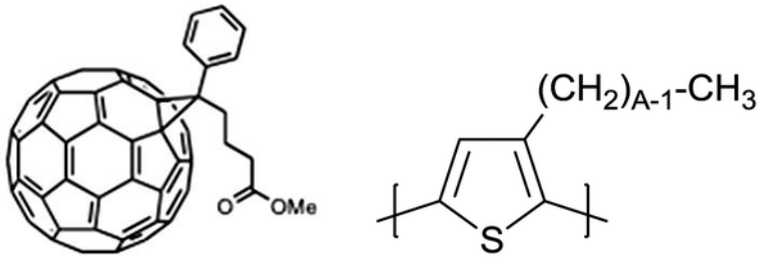

Figure 1. Chemical structures of [6,6]-phenyl-C_{61}-butyric acid methyl ester (PCBM) [14]and poly(3-alkylthiophene) (P3AT). [15]

PCBM and a fullerene (C60) were chosen for electron acceptor material and different kinds of P3ATs were prepared for electron donor material such as P3HT, P3NT, and P3DT. Using these materials, we built four donor-acceptor pair systems: C60-P3HT, PCBM-P3HT, PCBM-P3NT, and PCBM-P3DT. The weight ratio of all models was 1:1. All models consisted of 100 polymers chains with the degree of polymerization (DP) of 50 and the number of electron acceptor materials with the respective weight ratio.

MOLECULAR DYNAMICS SIMUATIONS AND EQUILIBRATION

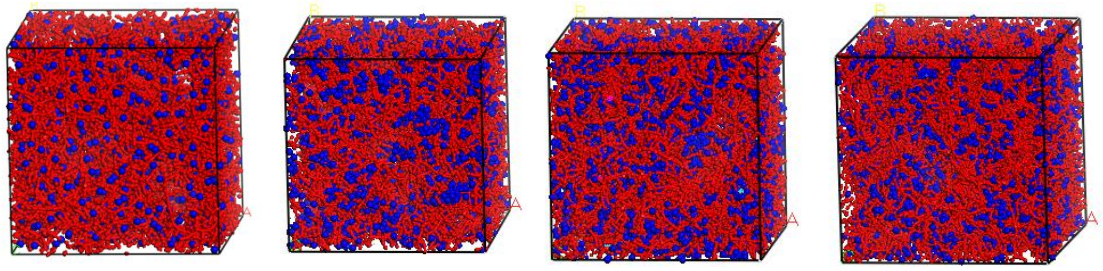

Figure 2. Morphologies of blends, (a) C_{60}-P3HT, (b) PCBM-P3HT, (c) PCBM-P3NT, and (d) PCBM-P3DT with ratio of 1:1.

Coarse-grained MD simulations were performed using Large-scale Atomic/Molecular Massively Parallel Simulator (LAMMPS) [16] software developed by Sandia National Laboratory, with newly developed coarse-grained force field. The equation of motion was integrated using the Verlet algorithm [17] with a time step of 2.0 fs. The Nose-Hoover thermostat (reference) for the isothermal-isobaric ensemble (NPT) simulations used a damping relaxation time of 0.1 ps and a dimensionless cell mass factor

of 1.0. Due to the thermodynamic stability of the structures, the initial structures underwent the mild annealing procedure. The annealing procedure utilizes a systematic variation of the temperature and volume to accelerate the equilibration.[18] First, the structures were gradually expanded while the temperature was gradually increased from 300 K to 500 K for 100 ps. Second, the canonical ensemble (NVT) MD simulation was implemented at 500 K for 200 ps. Next, the structures were cooled to 300 K and compressed to the desired density for 100 ps. This annealing step was performed repetitively for five times. Then, another NVT MD simulation was employed for 2 ns and NPT MD simulation was followed for 30 ns to equilibrate the structure fully.

CHAPTER 3

RESULT AND DISCUSSION

COARSE GRAINED FORCE FIELD DEVELOPMENT

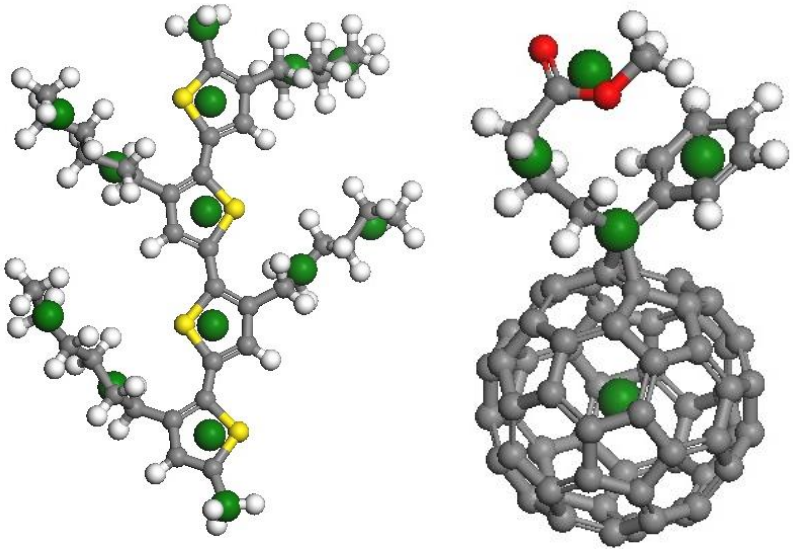

Figure 3. Atomistic models of P3HT and PCBM and the center of mass of each cluster, green beads.

Coarse-grained models for P3HT and PCBM were first developed as illustrated in Figure 3. The coarse-grained model proposed by Huang *et al[19]* was adopted for the P3HT. For example, fourteen coarse-grained beads were placed to describe a dimer unit of the P3HT, which consists of four 3-hexyl thiophenes terminated by two methyl groups. Four beads were assigned to the thiophene (C_4H_3S) backbone fragments while eight of them were used to describe the four hexyl tails in which each bead represents either a C_3H_6 or C_3H_7 fragment. The two methyl terminal groups were replaced with two pseudo-atoms. Five beads were prepared to develop the coarse-grained model for the P3HT. Three of them were assigned to thiophene (C_4H_3S), C_3H_6, and C_3H_7 fragments constituting the 3-hexylthiophene dimer and the rest were assigned to CH3 that finalize the polymer. Each of the fourteen coarse-grained beads were positioned at the center of the mass (COM) for each of the fragments, respectively. In a similar way, five coarse-

grained beads were prepared to express the PCBM molecule following the approach suggested by To *et al* [9].. A single bead is used for C_{60} and each C_2H_2 and C_2H_4 are grouped into a coarse grained bead because the shapes of both groups were formed by the sp3 C-C covalent bonds that rarely deformed during MD simulation. For the remaining hydrocarbons in the side chain, the ring, $C_6H_{5,}$ and carbonyl group, $COOCH_{3,}$ are mapped into each single bead.

Next, we followed two steps to develop our own coarse-grained force field parameters which could accurately describe the intramolecular and intermolecular interactions in the P3HT-P3HT, PCBM-PCBM, and P3HT-PCBM coarse-grained model pairs. As the first step, atomistic models with force field parameters were prepared for as reference models to reliably describe the intramolecular and intermolecular interactions. We therefore adopted the DREIDING force field parameters [10] for the intermolecular interactions in the atomistic P3HT-P3HT and PCBM-PCBM pairs as well as the intramolecular interactions in the atomistic models of P3HT and PCBM. The DREIDING force field is a general force field for nonmetallic main group elements such as carbon, nitrogen, oxygen, hydrogen and a few metals. [11] On the other hand, the DREIDING force field based intermolecular interactions in the full atomistic thiophene-fullerene pairs had not been well validated, and thereby we developed our own force field parameters for the pair. Specifically, the atomistic force field parameters associated with the intermolecular interactions in the atomistic thiophene-fullerene pairs were fit to describe the potential energy surfaces of the pairs.

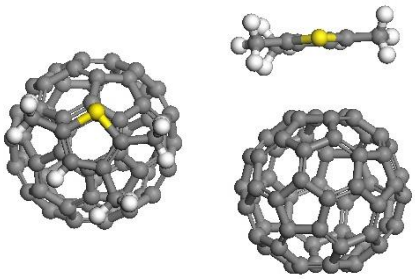

(a) Thiophene parallel to the pentagon of C_{60}

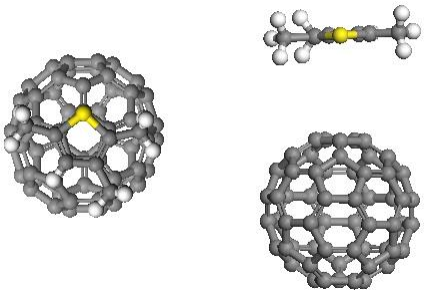

(b) Thiophene parallel to the hexagon of C_{60}

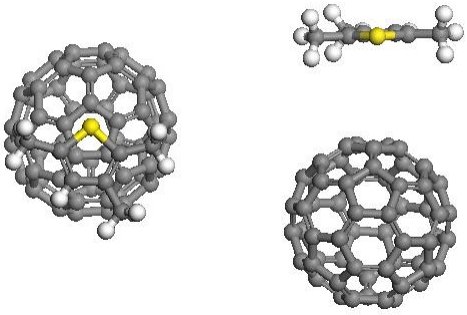

(c) Thiophene parallel to the center of hexagon of C_{60}

Figure 4. Top and side view of three different orientations of P3HT-PCBM pair in all atomistic models.

As shown in Figure 4, three conformations for the thiophene-fullerene pairs were intuitively considered for the force field fitting processes. Three configurations were chosen based on the geometry optimization trials. Thiophene in Figure 2(a) was parallel to the pentagon of the fullerene and thiophene in Figure 2(b) was parallel to the hexagon of the fullerene. In Figure 2(c), thiophene was parallel to the center of hexagon of C_{60}. To

fit the atomistic force field parameters, the Morse potential function was adopted and defined below:

$$V(r) = D_e\left(1 - e^{-a(r-r_e)}\right)^2 \quad (2)$$

where r (r_e) is an (equilibrium) distance between two atoms, D_e is the well depth, and a is related to the width of the potential function. Berry *et al.* [20] reported that the Morse potential function had the flexibility as compared with the Lennard-Jones potential function and thereby it allowed us to adjust the potential energy surfaces moderately realistic and flexible to describe the multi-dimensional surface. The resultant potential energy surface plots of Figure 4(a) predicted by both the DFT method and new force field are shown in Figure X. The new force field parameters and the plots of remainder models are shown in the Appendix.

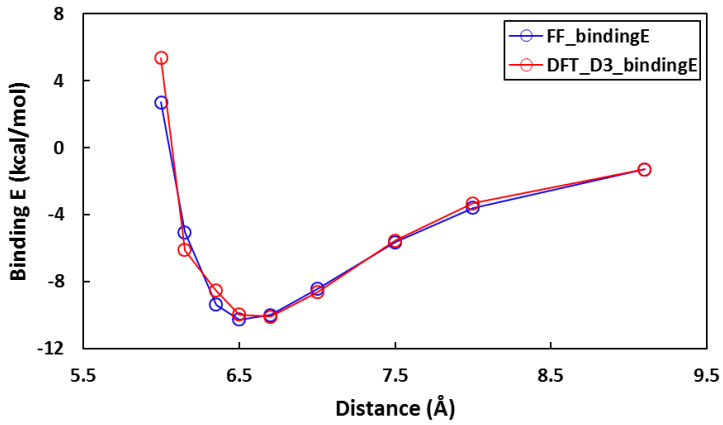

Figure 5. Potential energy surface plot of Figure 2(a)

According to Figure 5 and the Appendix, our atomistic force field parameters are well describing the potential energy surfaces.

In the second step, the coarse-grained force field parameters associated with the intermolecular interactions in the coarse-grained models of the P3HT-P3HT, PCBM-PCBM, and P3HT-PCBM pairs as well as the intramolecular interactions in the coarse-grained models of the individual P3HT and PCBM were obtained to accurately mimic the potential energy curves associated with their atomistic models. The conformational variations for P3HT-P3HT, PCBM-PCBM, and P3HT-PCBM were intuitively considered

for the coarse grained force field fitting process. All conformations are shown in the Appendix. The potential function which was utilized to fit the coarse-grained force field parameters is defined below.

$$V = \sum_{bonds} \frac{1}{2} k_{bond}(r - r_e)^2 + \sum_{angles} \frac{1}{2} k_{angle}(\theta - \theta_0)^2 + \sum_{torsions} \frac{1}{2} k_{torsion}\big(1 + \cos(n\varphi_0 - d)\big) + \sum_{coulomb}^{i<j} \frac{q_i q_j}{r_{ij}} + \sum_{vdW} D_e\big(1 - e^{-a(r-r_e)}\big)^2 \quad (3)$$

where $k_{bond}, k_{angle}, and\ k_{torsion}$ are force constants in bond, angle and torsion, r_e is the equilibrium length, θ_0 is the equilibrium angle, φ_0 is the equilibrium angle, n is periodicity, d is either +1 or -1, $q_i\ and\ q_j$ are charges in electron units, r_{ij} is the distance between i and j atoms. Regarding the intramolecular interactions, harmonic potential functions were utilized to describe the bond stretch and angle bending energies while the dihedral potential function was utilized to express the torsional energy. It is worthwhile to note the Morse potential function was again used to express the intermolecular van der Waals interactions. For the electrostatic interactions, the summed charges of the atoms contained in individual coarse-grained beads were close to zero and thereby the Coulombic interaction term was ignored. The potential energy surface plots of the PCBM-P3HT case predicted by the fitted coarse grained force field parameters are shown in Figure 6 and the coarse grained force field parameters and the remainder of bond energy curves are shown in the Appendix.

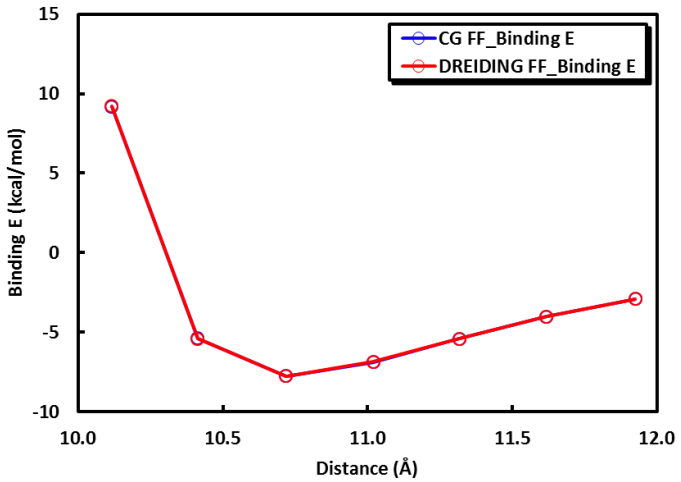

Figure 6. PCBM-P3HT Potential energy surface plot of Figure 8(a) in Appendix

According to the potential energy surface plot in Figure 6 and the Appendix, our coarse grained force field parameters are well reproducing the potential energy surfaces of the atomistic force field.

COARSE GRAINED FORCE FIELD VALIDATION

As compared with full atomistic models, coarse-grained models enable us to efficiently perform macroscopic simulations in a shortened time.[21, 22] Despite this advantage of the coarse-grained models, the questions on their reliability arising from the beads replacing molecular fragments without any chemical intuition need to be answered for further investigations. In the following content, our coarse-grained models on P3HT and PCBM were validated by comparing coarse-grained MD simulation results with our atomistic MD simulation results as well as relevant experimental results.

Physical properties

To validate our coarse-grained models, we first prepared for two coarse-grained models containing 10 polymer chains of P3HT with the DP of 50 and 100 PCBM molecules. Two atomistic models containing P3HT and PCBM, whose size is equivalent to the coarse-grained models, were also prepared as reference models. The MD simulations for both schemes were then performed to predict their system densities and solubility parameters. The DREIDING force field parameters were employed to describe

the interactions of particles in the atomistic models while the developed coarse-grained force field parameters were used to describe the interactions of beads constituting the coarse-grained models. Note that amorphous structure models of PCBM and P3HT mixtures in this work were utilized to perform the MD simulations. It is also worthwhile to note that the annealing and equilibration time scales for P3HT were longer than those for PCBM due to the poor miscibility in organic materials arising from the polymer rigidity. The detailed MD simulation based analyses on two representative physical properties, namely density and solubility parameter, to validate our coarse-grained models are described below.

Table 1. Experiment and simulated density of PCBM and P3HT

	Density of PCBM(g/cm^3)	Density of P3HT(g/cm^3)
Experiment	1.50[24]	0.94[19]
Atomistic Model	1.46	0.71
Coarse-grained Model	1.47	0.82

The first physical property, namely density, was predicted for each of the models by analyzing the MD simulation results and the corresponding values are listed in Table 1. Their experimental densities are tabulated along the simulation values for comparison, as well. As seen in Table 1, the densities of the coarse-grained models were estimated to be 0.82 g/cm^3 and 1.47 g/cm^3 for P3HT and PCBM, respectively, which were significantly close to the atomistic model densities of 0.71 g/cm^3 and 1.46 g/cm^3 for P3HT and PCBM, respectively. This is reasonable in the sense that the interaction parameters of particles in the coarse-grained models were developed to describe potential energy surfaces of the full atomistic models. The reported experimental densities for P3HT and PCBM were 0.94 g/cm^3 and 1.50 g/cm^3 and they were slightly higher than the simulated densities. The deviation in the densities of P3HT can be understood by the

structural differences between the experimental samples and simulation models.[23] In other words, it is generally expected that the perfectly amorphous polymer structures described in the simulations models will have less densities than the experimental polymer structures containing not only the amorphous polymer chains but also the crystalline polymer chains. Nevertheless, in general sense, the results of full atomistic and coarse-grained models are in good agreement with the experiment data, exhibiting better match with the coarse-grained models than the full atomistic models.

Solubility parameter

The other physical property which could be determined by the MD simulations is the solubility parameter. The solubility parameter of a model system is defined by the squared root form of the cohesive energy density which is described as

$$\delta = \sqrt{\frac{\Delta E_p}{V}} \ . \tag{4}$$

where ΔE_p is the cohesive energy density and V is the volume of the equilibrated model system.

$$\Delta E_p = E_{total} - n_{chain} \times E_{single\ chain}. \tag{5}$$

The cohesive energy density of the P3HT (PCBM) model system was simply estimated by examining the difference in the potential energies between a model containing 10 P3HT chains with the DP of 50 (100 PCBM molecules) and a model containing isolated 1 P3HT chain with the same DP (1 PCBM molecule). The solubility parameters were predicted by introducing the resultant cohesive energy densities into the Equation (4).

Table 2. Experiment and simulated solubility parameters of PCBM and P3HT

	PCBM(Mpa)$^{1/2}$	P3HT(Mpa)$^{1/2}$
Experiment	5.2[25]	12.8 - 20[26]
Atomistic	8.01	28.9
Coarse-grained	5.7	11.7

The resultant simulated solubility parameters with reported experimental values are listed in Table 2. It is quite clear from the table that the simulated solubility parameters (11.7 for P3HT and 5.7 for PCBM) for the coarse-grained models of P3HT and PCBM agreed well with the experimental solubility parameters.

In conclusion, our coarse grained force field parameters are accurately mimicking the potential energy surface of the reference energy surface. Also, such good agreements between simulation and experimental results on the physical properties, namely density and solubility parameter, suggest that the developed coarse-grained models are reliable for further investigations.

MORPHOLOGICAL PROPERTIES

To study the morphological properties, the pair correlation function (PCF) and interface to volume ratio are calculated. The pair correlation function is a method to analyze the morphology in microscopic scale since it shows the distribution of neighboring molecules from a particular particle or molecule that surrounds a molecule. Likewise, the interfacial area to volume ratio, γ, is another good indicator for estimating efficient exciton dissociation and understanding the morphology of the active layer in macroscopic scale. [5] In this section, we analyze the morphology of each model in both microscopic and macroscopic scales and find the connection to the efficiency of the organic photovoltaics.

DISTRIBUTION OF DONOR AND ACCEPTOR

The exciton is produced by the light travels along the electron donor and the exciton is released from the donor. Electrons are absorbed by the electron acceptor, a fullerene, and electrons diffuse to the electrode along fullerene. Also, holes are transported through the donor to the electrodes. [1] Therefore, the distribution of donor-donor and acceptor-acceptor determines that the system carries a good pathway for electrons and holes to the each electrode. The distribution of donor-acceptor determines the degree of the exciton dissociation at the interface in the microscopic scale.

To investigate the distribution of each pair, the pair correlation function (PCF), a time-averaged probability of finding molecules at distance r from another molecule, is calculated. The pair correlation function is calculated using the equation below.

$$g_{pair}(r) = \left(\frac{n_{pair}}{4\pi r^2 \Delta r}\right) / \frac{N_s}{V} \quad (6)$$

where n_{pair} is the number of atoms in each pair located at a distance r in a shell of thickness Δr from each atom, N_s is the total number of atoms in the system, and V is the total volume. For the direct comparison, the quantity of $g(r)$ is multiplied with the number density of molecules in a unit cell system. [18] Figure X shows the pair correlation, $g_{pair}(r)$, for each model below.

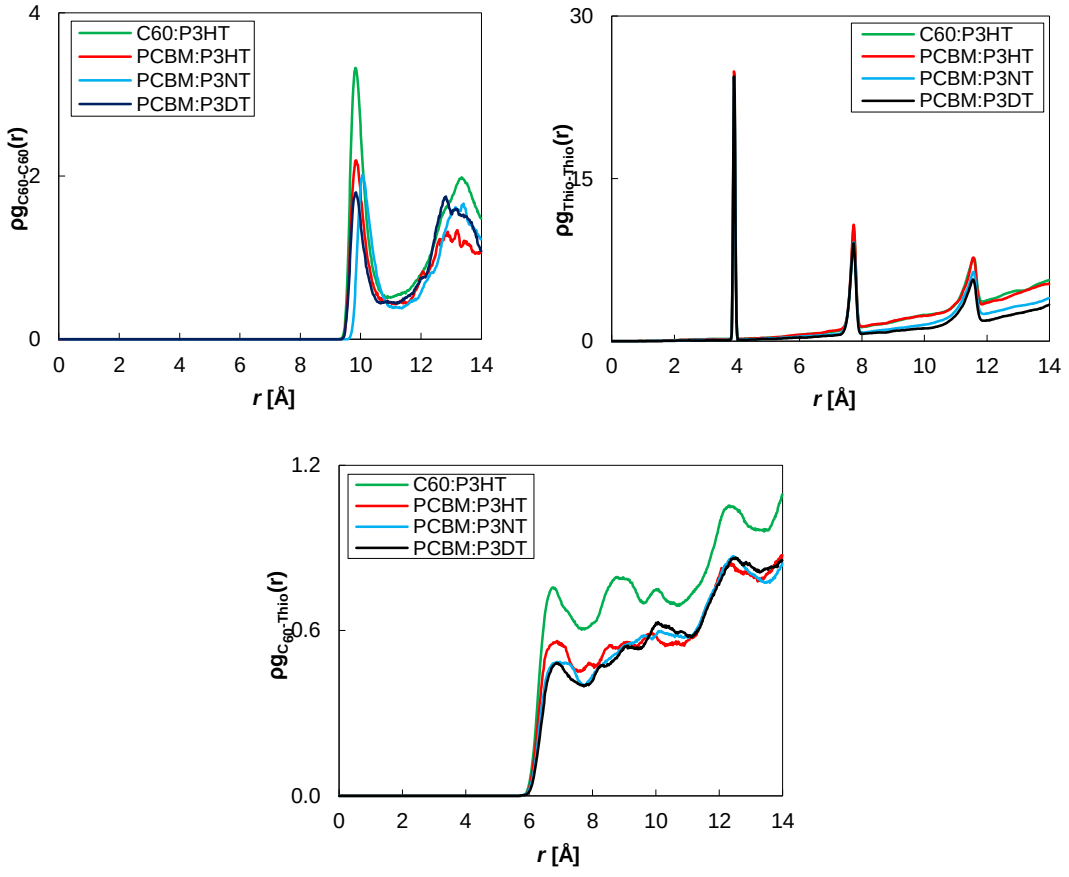

Figure 7. Pair correlation function (a) C_{60}-C_{60}, (b) Thiophene-Thiophene, and (c) C_{60}-Thiophene

To quantify the distribution of each case, the coordination number (CN) is calculated by integrating the first peak of each model and it is shown in Table X.

Table 3. Coordination number

	Pair		
Model	C_{60}-C_{60}	Thio-Thio	C_{60}-Thio
C_{60}-P3HT	2.28	2.43	1.26
PCBM-P3HT	1.79	2.41	0.99
PCBM-P3NT	1.45	2.22	0.68
PCBM-P3DT	1.40	2.18	0.65

In Figure 7(a), the C_{60}-C_{60} PCF is shown and the first peak of all models is observed within the range from 10 Å to 11 Å for all models. The CN of C60-P3HT (2.28) is the largest among the models and this indicates that fullerenes are closely packed around other fullerenes in C60-P3HT. Since the size of C_{60} is smaller than PCBM, fullerenes are likely to be found near each other. Among PCBM-polymer combinations, PCBM-P3HT is the highest in not only the first peak but also the CN. This indicates that the electron transportation in PCBM-P3HT occurs more efficiently than other pairs and the side chains of polymer distract the close distribution of PCBM. The PCF of thiophene-thiophene is shown in Figure 7(b). Three peaks are shown in the range of 14Å and the first two peaks, at 4Å and 8Å, show more likely the intramolecular distribution, the distance within the polymer chains, not intermolecular distribution. It is difficult to discriminate between intermolecular and intramolecular distribution using Cerius^2.[27] In Figure 7(c), the C_{60}-thiophene PCF is shown. The distribution of C60-thiophene relates to the efficient exciton dissociation in the microscopic scale. The greater number of a thiophene molecule around C_{60} leads to the better chance to dissociate the exciton efficiently. In the PCF of the C_{60}-thiophene, several peaks with different intensity are observed. In this case, we picked the first peak that showed the highest intensity and analyzed because the higher intensity implies a greater chance of a molecule being

located at the specific distance from fullerene. According to Figure X(c) and Table X, C_{60}-P3HT shows not only the highest peak in the PCF of C_{60}-thiophene but also the coordination number (1.26). As we discussed in the PCF of C_{60}-C_{60}, the size of C_{60} enabled to gather molecules closely and this affected the packed distribution, also. For PCBM-polymer pairs, PCBM-P3HT exhibited the highest peak in the PCF and the largest in the coordination number. Overall, C_{60}-P3HT shows the highest distribution in donor-donor, acceptor-acceptor and donor-acceptor. This combination may result in creating a pathway to each electrode within the domain and each atom is able to dissociate the exciton efficiently in the microscopic scale.

INTERFACE TO VOLUME RATIO

The interface of electron donor-acceptor to volume ratio, γ, is a good indicator of the exciton dissociation in the macroscopic scale and the ratio of the blend has to be large for efficient exciton dissociation.[5] The ratio was calculated by the equation below.

$$\gamma = A_{interface}/V_{box} \tag{7}$$

where $A_{interface}$ is the total interfacial area and V_{box} is the volume of the simulation box. To characterize the total interfacial area, *A*, the Connolly surface were performed to calculate the electron donor and acceptor interfacial area with Materials Studio by *Accelrys*.[28] The Connolly surface area can be obtained from the bottom of a probe molecule rolling across the surface. [29] The definition of the Connolly surface is shown in Figure 8.

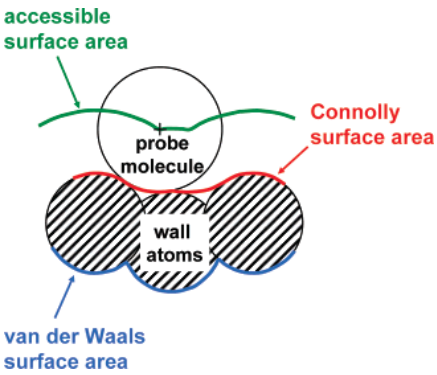

Figure 8. Definition of the accessible surface area (green line), the Connolly surface area (red line), and the van der Waals surface area (blue line).[29]

The probe size and van der Waals scale factor are critical for the accuracy of calculation. Among the donor and acceptor materials, we focused on PCBM which was the path of the electrons. We first removed polymers in the box and disconnected all bonds of PCBM. To calculate the van der Waals scale factor, the probe size was calculated from the radius of gyration of all atomistic PCBM. With the obtained probe size, van der Waals scale factor that described the volume of PCBM was adjusted. Then, the probe sizes of each model were varied because they were based on the bond distance that enabled to connect all disconnected atoms. The probe size and vdW scale factor are shown in Table 4. We picked the last 10 ns at the equilibration steps and the interface to volume ratio of each model over the time is shown below in Figure 9.

Table 4. The Connolly surface information

Model	Bond distance (Å)	Probe size (Å)	vdW Scale Factor
C60-P3HT	15	7.75	1.45
PCBM-P3HT	10	5.25	1.56
PCBM-P3NT	11	5.75	1.56
PCBM-P3DT	11	5.75	1.56

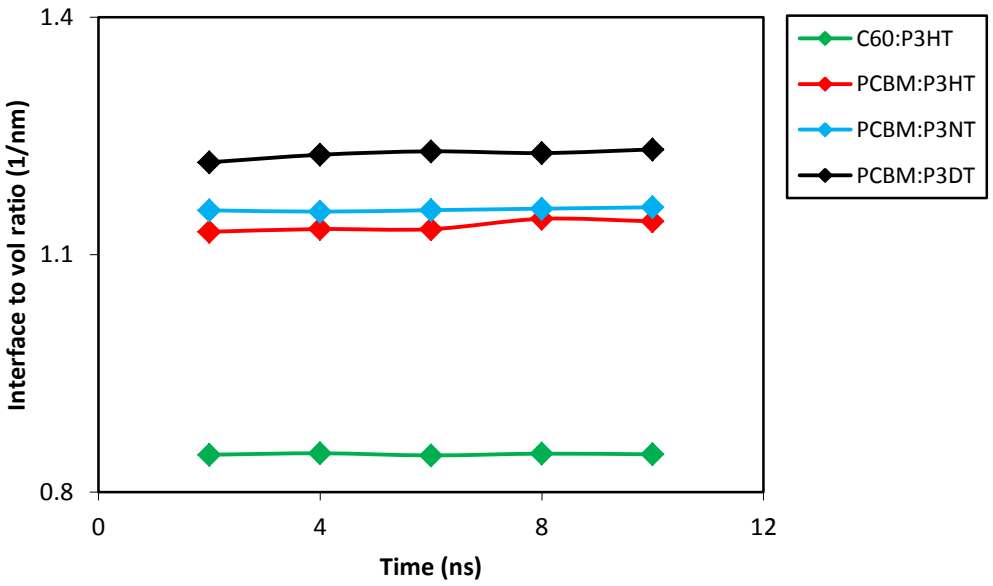

Figure 9. Interface to volume ratio over the time.

The interface to volume ratio exhibits different trends comparing to the pair correlation function and the coordination number. C_{60}-P3HT is the highest coordination number at the donor-acceptor interface but the pair exhibits the lowest interface to volume ratio. The low interfacial area comes from the limited solubility in organic solvents[30] and it causes a severe decrease in the exciton dissociation. Therefore, C60 cannot be a good candidate for improving the efficiency of organic photovoltaics. For PCBM-polymer pairs, the interfacial area of electron donor and acceptor increases as the length of the side chain grows. The interface to volume ratio of PCBM-P3DT is the largest (1.23) comparing to that of PCBM-P3HT (1.13) and PCBM-P3NT (1.16). Since the results are in the order of the length of the side chain, the longer side chains aid to achieve the bigger interfacial area. Hence, PCBM-P3DT exhibits the most efficient exciton dissociation in the macroscopic scale.

TOTAL C_{60}-THIOPHENE PAIRS PER UNIT VOLUME

According to the coordination number, C60-P3HT shows the highest distribution between electron donor and acceptor materials in the microscopic level but its interface to volume ratio, the macroscopic scale, is the lowest. Although a selected atom is surrounded by large number of atoms, it does not necessarily lead to the high interfacial area. C60-P3HT exhibited the packed distribution but the interfacial area was significantly small due to the low miscibility in the organic materials. On the other hand, PCBM-P3DT shows the highest interface to volume ratio but the distribution of electron donor and acceptor is the lowest. If the distribution between donor and acceptor were low, the efficiency could be affected whether the interfacial area is large or small. To satisfy the both microscopic and macroscopic scale, we calculated the total C_{60}-thiophene pair per unit volume. The equation is shown below.

$$Total\ C_{60} - Thiophene\ Pairs\ per\ Unit\ Volume = \sum_i \gamma_i * CN \quad (8)$$

where γ_i is interface to volume ratio over the time and *CN* is the coordination number. We calculated ε and the result is show in Figure 10 below.

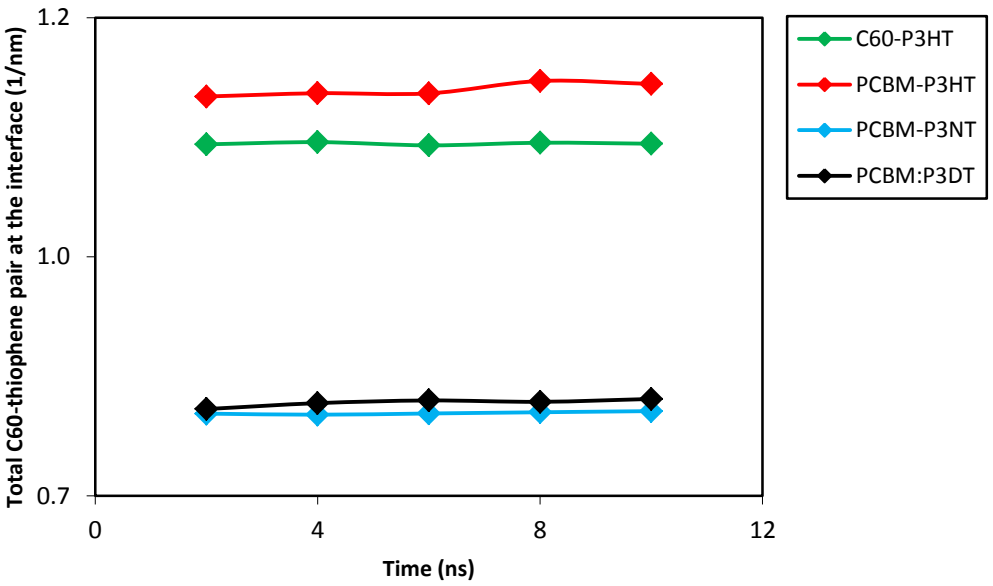

Figure 10. Total C_{60}-thiophene pair per unit volume

Though the interface to volume ratio of PCBM-P3DT was the highest than others, the total C_{60}-thiophene pair per unit volume of the pair was significantly decreased due to the low distribution. For C60-P3HT, the interface to volume ratio was significantly low but the total C_{60}-thiophene pair per unit volume ranked the second due to the most packed distribution in C_{60}-thiophene. Among the pairs, PCBM-P3HT satisfies both microscopic and macroscopic criteria. In PCBM-P3HT system, C60 and thiophene are relatively well distributed within the system and the pair would exhibit good exciton dissociation at the active layer based on the interface to volume ratio. Therefore, PCBM-P3HT is the optimum electron acceptor and donor materials among compared pairs.

CHAPTER 4

CONCLUSIONS

We developed the new coarse grained force field parameters to study the morphological properties that affect the efficiency of the organic photovoltaics. We adopt a generic force field, the DREIDING force field, and implemented the DFT calculation in order to describe the intermolecular interaction that the DRIEDING force field did not offer. Based on the reliable atomistic force field, the coarse grained force field parameters also developed. The potential energy surfaces of both intramolecular and intermolecular interaction are well described. Then, the validations of the coarse grained model force field were performed. We compared the simulated results to experimental results such as density and solubility parameter and the results were in good agreements. Then, we constructed the coarse grained models using four different combinations of electron acceptor and donor materials to analyze the morphological properties in the microscopic and macroscopic scales that related to the efficiency of the organic photovoltaics. The PCF of electron donor and acceptor materials was implemented and the coordination number was calculated to quantify the distribution. They quantify the distribution of molecules that surrounds a molecule. Through the distribution analysis, C_{60}-P3HT exhibited the highest distribution in donor-donor, acceptor-acceptor and donor-acceptor. To quantify the morphological properties in the macroscopic scale, the interface to volume ratio was calculated by using the Connolly surface. Though C_{60}-P3HT was superior to other cases in the microscopic scale, it shows the lowest interface to volume ratio due to its limited solubility in organic materials. In the macroscopic scale, PCBM-P3DT is the best in the interface to volume ratio and the longest side length improves the interfacial area. From the morphological quantities above, we see the different trends in the microscopic and macroscopic scale. Therefore, we calculated the total C_{60}-thiophene pair per unit volume to find the link between the microscopic and macroscopic scales.

Unlike the individual results in each scale, PCBM-P3HT satiefied both scales. C_{60}s are well spread-out around a thiophene within the system and the interfacial area is relatively high. Therefore, PCBM-P3HT is the best combination that satisfies both microscopic and macroscopic scales among the pairs we compared.

We made great efforts to develop the robust coarse grained force field since it was the first step in the molecular dynamics simulation. From the validation of the force field, we realized that our force field is describing the potential energy surface well. Due to the time limitation, we could analyze some morphological properties such as the PCF, CN, interface to volume ratio and the total C_{60}-thiophene per unit volume. With our reliable force field, we would be able to do other morphological properties that we have not done yet. Also, we could do simulations to analyze the mechanical properties for the stability and durability of the cell. In addition, if we collaborated with the group that did the experiment on organic photovoltaics, we would obtain more qualitative analysis. In the future, we would like to study other morphological properties in the active layer and the properties of the cell using molecular dynamics simulations.

APPENDIX A

FORCE FIELD FITTING

Atomistic force field parameterization

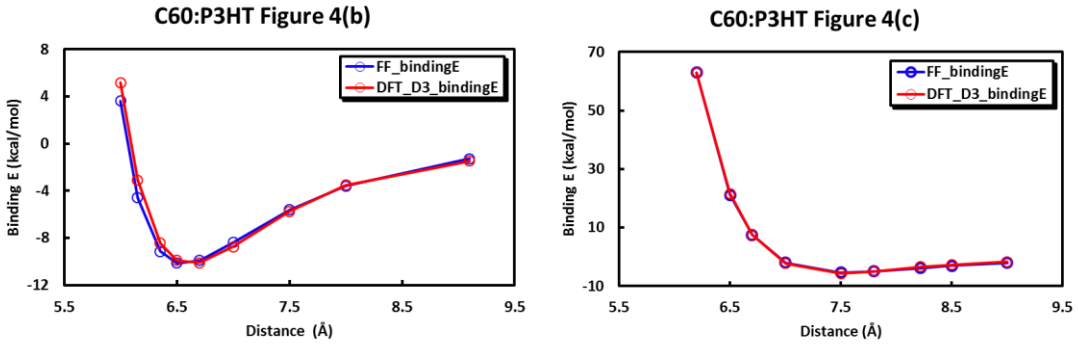

Figure 11. Potential energy surface

Table 5. Atomisic force field parameters (Non-bonded interaction)

Molecule	Parameter	C_C60
S_Th	D [kcal/mol]	0.215
	re [Å]	3.584
	a	2.114
	gamma	15.156
C_Th	D [kcal/mol]	0.014
	re [Å]	3.912
	a	1.913
	gamma	14.967
C_3Th	D	0.304
	re	3.822
	a	1.012
	gamma	7.732
H_Th	D	0.016
	re	3.538
	a	1.852
	gamma	13.108

Coarse grained force field parameterization

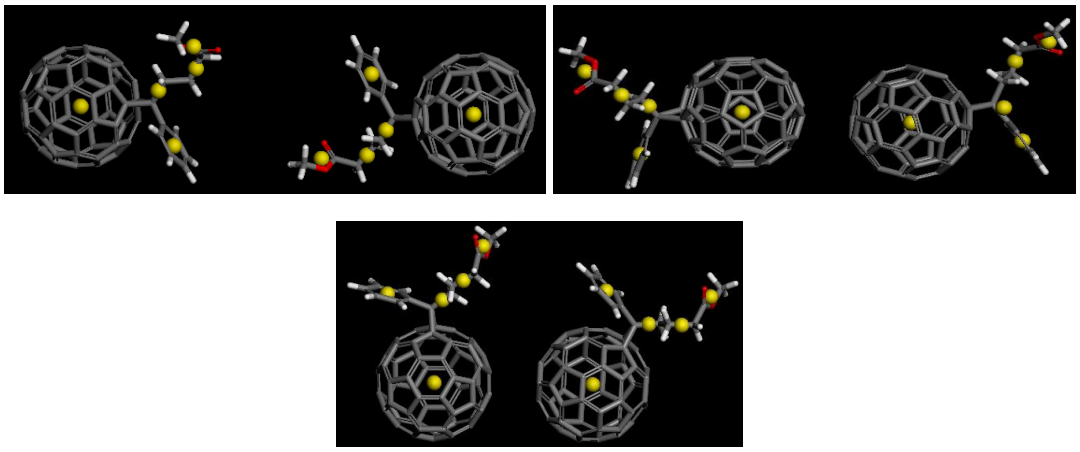

Figure 12. PCBM-PCBM conformations for CG FF parameterization, from the top left, (a), (b) and (c)

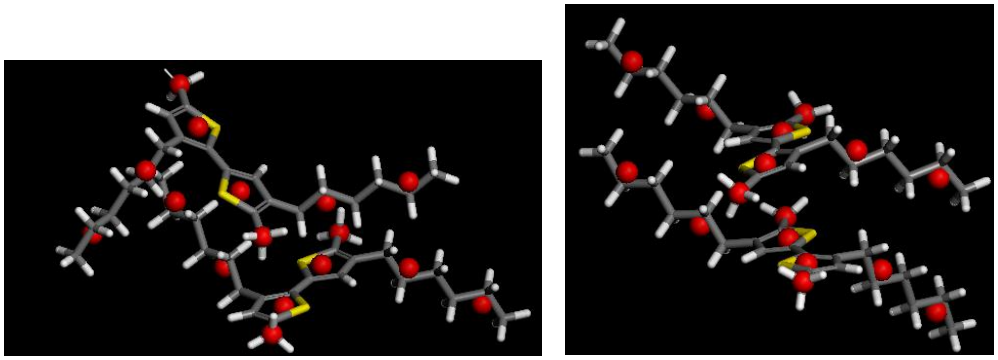

Figure 13. P3HT-P3HT conformations for CG FF parameterization, from the left, (a) and (b)

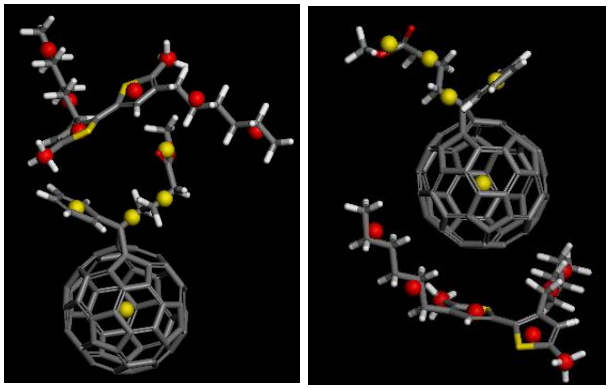

Figure 14. PCBM-P3HT conformations for CG FF parameterization, from the left, (a) and (b)

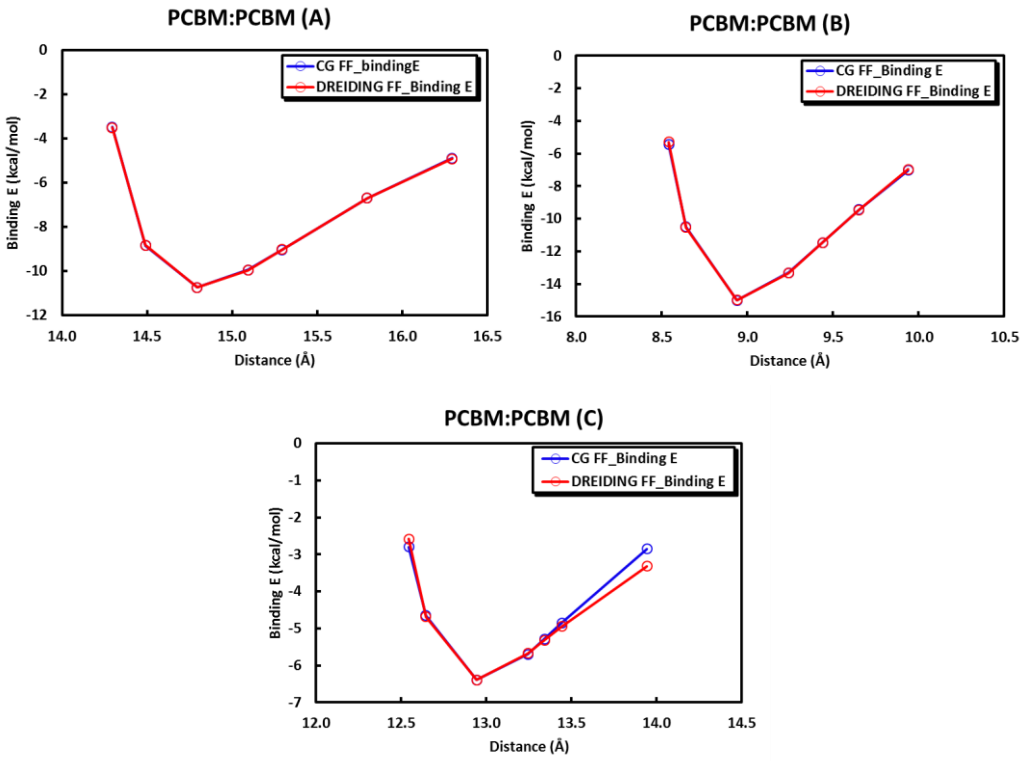

Figure 15. Potential energy surfaces of PCBM-PCBM

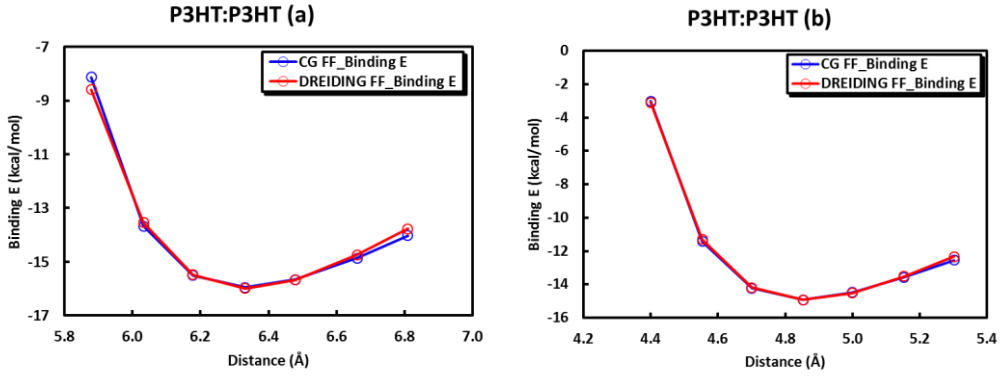

Figure 16. Potential energy surfaces of P3HT-P3HT

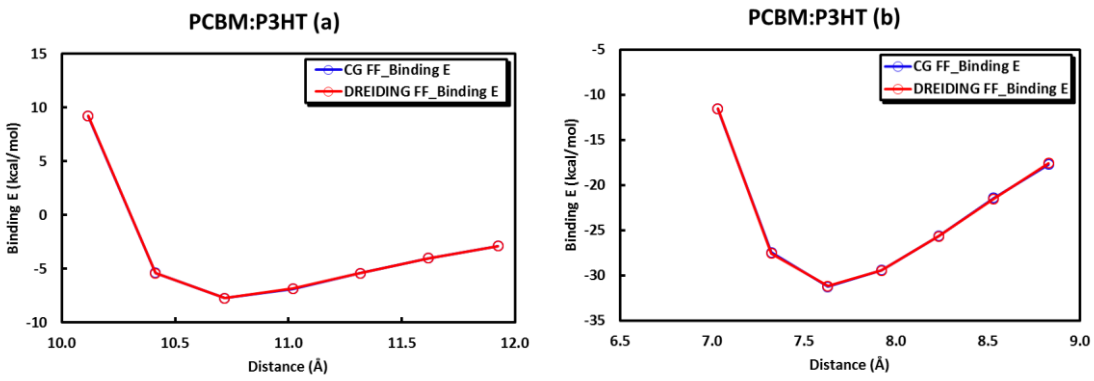

Figure 17. Potential energy surface of PCBM-P3HT

Table 6. Coarse grained force field parameters of PCBM-PCBM

Molecule	Parameter	C_C60	C6H5	C2H2	C2H4	COOCH3
C60	D [kcal/mol]	6.4642	8.7045	0.0136	0.6049	7.0291
	re [Å]	9.9578	6.1389	7.5000	6.0536	8.8617
	a	1.3865	7.7380	3.3447	6.2141	2.2251
	Gamma	27.6126	95.0055	50.1706	75.2354	39.4354
C6H5	D [kcal/mol]		8.1483	0.0839	4.1584	0.5114
	re [Å]		3.8660	3.8000	4.2308	4.8966
	a		1.3858	8.5502	0.8549	1.6125
	Gamma		10.7150	64.9815	7.2337	15.7919
C2H2	D [kcal/mol]			1.5433	6.6357	0.0004
	re [Å]			3.6570	3.3925	5.0199
	a			4.5161	5.8360	2.5808
	Gamma			33.0311	39.5970	25.9109
C2H4	D [kcal/mol]				1.0144	0.3769
	re [Å]				3.7530	4.0085
	a				2.1310	0.0000
	Gamma				15.9955	0.0002
COOCH3	D [kcal/mol]					7.8621
	re [Å]					3.8660
	a					1.0871
	Gamma					8.4058

Table 7. Coarse grained force field parameters of P3HT-P3HT

Molecule	Parameter	Thiophene	C3H6	C3H7	CH3
Thiophene	D [kcal/mol]	0.8667	3.8812	0.0239	0.0028
	re [Å]	4.5000	4.2877	6.9283	4.8000
	a	0.3889	1.1228	0.0946	3.2747
	Gamma	3.5001	9.6284	1.3109	31.4372
C3H6	D [kcal/mol]		1.5332	0.0258	0.0015
	re [Å]		5.3162	5.1292	8.1490
	a		1.9386	0.1682	0.0241
	Gamma		8.6863	3.7603	0.3883
C3H7	D [kcal/mol]			1.2535	0.0255
	re [Å]			4.1992	10.1020
	a			0.8754	0.0904
	Gamma			1.9192	0.2460
CH3	D [kcal/mol]				0.9815
	re [Å]				1.7896
	a				8.9519
	Gamma				28.2192

Table 8. Coarse grained force field parameters of PCBM-P3HT

Molecule	Parameter	C_C60	C6H5	C2H2	C2H4	COOCH3
Thiophene	D [kcal/mol]	8.3041	0.0542	1.3154	0.5462	2.5842
	re [Å]	6.9436	5.1400	3.6292	3.7178	4.1471
	a	0.7907	2.7255	2.0004	2.0032	1.6024
	Gamma	10.9807	28.0187	14.5198	14.8954	13.2908
C3H6	D [kcal/mol]	9.2633	1.0626	0.5674	3.6105	0.0028
	re [Å]	6.9371	3.9400	4.2426	4.5346	4.5911
	a	1.3634	1.9980	1.0307	0.9695	1.1043
	Gamma	18.9161	15.7443	8.7458	8.7925	10.1397
C3H7	D [kcal/mol]	1.9014	1.0680	1.0304	0.2194	0.2945
	re [Å]	8.0742	4.0587	3.3537	3.8179	4.9391
	a	0.4783	1.6472	0.4968	0.9921	0.9991
	Gamma	7.7241	13.3710	3.3319	7.5756	9.8691
CH3	D [kcal/mol]	1.0097	3.3401	0.4192	0.2263	0.0233
	re [Å]	7.9790	3.9976	2.7321	2.7757	2.6167
	a	0.6437	1.3470	1.9066	1.0126	1.0043
	Gamma	10.2722	10.7697	10.4181	5.6216	5.2558

Table 9. Bond Stretching parameters

Force Field Type	k (kcal/mol)	r_0 (Å)
CH_3C - Thio	679.91	2.826
CH_3F - Thio	683.75	2.796
C_3H_6 - C_3H_6	454.23	3.593
Thio - C_3H_7	655.26	3.941

Table 10. Angle bending parameters

Force Field Type	k (kcal/mol)	θ (Degree)	Radian
CH_3C - Thio - C_3H_6	608.61	69.28	1.21
CH_3F - Thio - C_3H_6	521.69	125.96	2.20
CH_3C/F - Thio - Thio	562.13	165.44	2.89
Thio - C_3H_6 - C_3H_6	428.07	154.16	2.69
C_3H_6 - C_3H_6 - C_3H_7	321.9	167.86	2.93
Thio – Thio - C_3H_7	742.93	114.82	2.00
CH_3C – Thio - C_3H_7	839.95	72.48	1.27
CH_3F – Thio - C_3H_7	683.17	128.57	2.24
C_3H_6 - C_3H_6 - C_3H_6	469.01	154.25	2.69

Table 11. Torsion parameters

Force Field Type	k (kcal/mol)	ϕ (Degree)	Radian
CH_3C - Thio - C_3H_6 - C_3H_7	25.58	97.20	1.70
CH_3C - Thio - Thio - CH_3F	1.43	166.62	2.91
CH_3C - Thio - Thio - C_3H_6	1.41	8.46	0.15
Thio -Thio - C_3H_6 - C_3H_7	1.55	87.08	1.52
CH_3F - Thio - Thio - C_3H_6	2.01	24.88	0.43
CH_3F - Thio - C_3H_6 - C_3H_7	20.43	86.28	1.51
C_3H_6 - Thio - Thio - C_3H_6	47.96	181.55	3.17
CH_3F - Thio - Thio - Thio	1.8	191.25	3.34
C_3H_6 - Thio - Thio - Thio	40.58	23.25	0.41
Thio - Thio - Thio - Thio	6.01	185.94	3.25
CH_3C - Thio - Thio - Thio	1.35	154.73	2.70
C_{60} - C_2H_2 - C_2H_4 - $COOCH_3$	1.00	125.74	2.19
C_6H_5-C_2H_2-C_2H_4-$COOCH_3$	0.94	225.90	4.47
Thio-C3H6-C3H6-C3H7	1.73	157.7	2.75
Thio-Thio-C3H6-C3H6	1.55	87.08	1.52
CH3C-Thio-C3H6-C3H6	25.58	97.20	1.70
CH3F-Thio-C3H6-C3H6	20.43	86.28	1.51
C3H7-Thio-Thio-C3H7	3.86	145.052	2.53
Thio-Thio-Thio-C3H7	4.473	24.83	0.43
CH3-Thio-Thio-C3H7	8.53	97.20	1.70
Thio-C3H6-C3H6-C3H6	1.08	145.05	2.53
C3H6-C3H6-C3H6-C3H7	1.73	157.7	2.75

REFERENCES

[1] Katherine A. Mazzio, C.K.L., *The future of organic photovoltaics.* The Royal Society of Chemistry, 2014. **44**: p. 78-90.

[2] G. Yu, J.G., J. C. Hummelen, F. Wudl and A. J. Heeger, Science, 1995. **270**: p. 1789-1791.

[3] Xiaoniu Yang, J.L., Sjoerd C. Veenstra, Wiljan J. H. Verhees, Martijn M. Wienk, Jan M. Kroon, Matthias A. J. Michels, and Rene A. J. Janssen, *Nanoscale Morphology of High-Performance Polymer Solar Cells.* Nano Letters, 2005. **5**(4): p. 579-583.

[4] Minh Trung Dang, L.H., and Guillaume Wantz, *P3HT:PCBM, Best Seller in Polymer Photovoltaic Reserach.* Advanced Materials, 2011. **23**: p. 3597-3602.

[5] Cheng-Kuang Lee, C.-W.P., Chih-Wei Chu, *Multiscale molecular simulations of the nanoscale morphologies of P3HT:PCBM blends for bulk heterojunction organic photovoltaic cells.* Energy & Environmental Science, 2011. **4**: p. 4124-4132.

[6] S.H. Lee, D.H.K., J.H. Kim, G.S. Lee, and J.G. Park, Journal of physical Chemistry C, 2009. **113**(52): p. 21915-21920.

[7] Tayebeh Ameri, N.L.a.C.J.B., *Highly efficient organic tandem solar cells: a follow up review.* The Royal Society of Chemistry, 2013. **6**: p. 2390-2413.

[8] A. Swinnen, I.H., P. Vanlaeke, J. D'Haen, J. Poortmans, M. D'Olieslaeger, and J. V. Manca, *Dual crystallization behaviour of polythiophene/fullerene blends.* The European Physical Journal Applied Physics, 2006. **36**: p. 251-256.

[9] Adams, T.T.T.a.S., *Modelling of P3HT:PCBM interface using coarse-grained forcefield derived from accurate atomsitic forcefield.* Physical Chemistry Chemical Physics, 2014. **16**: p. 4653-4663.

[10] Stephen L. Mayo, M.D.O., William A. Goddard III, *DREIDING: A Generic Force Field for Molecular Simulations.* Journal of Physical Chemistry, 1990. **94**: p. 8897-8909.

[11] Rakwoo Chang, A.V., *Insights into the Effect of Combustion-Generated Carbon Nanoparticles on Biological Membranes: A Computer Simulation Study.* Journal of Physical Chemistry B, 2006. **110**: p. 5073-5083.

[12] Stefan Grimme, J.A., Stephan Ehrlich, Helge Krieg, *A consistent and accurate ab initio parametrization of density functional dispersion correction (DFT-D) for the 94 elements H-Pu.* The Journal of Chemical Physics, 2010. **132**: p. 154104-1-1504104-19.

[13] Soonchul Kwon, J.I.C., Seung Geol Lee, Seung Soon Jang, *A density functional theory (DFT) study of CO_2 adsorption on Mg-rich minerals by enhanced charge distribution.* Computational Material Science, 2014. **95**: p. 181-186.

[14] Synchrotron, T.E., *Organic photovoltaics in situ annealing studied by grazing-incidence diffraction*. 2011.

[15] Wouter Dierckx, W.D.O., Jean-Christophe Bolsée, Wouter Maes, Dirk Vanderzande and Jean Manca, *Poly(3-alkylthiophene) nanofibers for optoelectronic devices.* Journal of materials Chemistry C, 2014. **2**: p. 5730-5746.

[16] Plimpton, S., *Fast Parallel Algorithms for Short-Range Molecular Dynamics.* Journal of Computational Physics, 1995. **117**: p. 1-19.

[17] William C. Swope, H.C.A., Peter H. Berens and Kent R. Wilson, *A computer simulation method for the calculation of equilibrium constants for the formation of physical clusters of molecules: Application to small water clusters.* Journal of Chemical Physics, 1982. **76**: p. 637-649.

[18] Khaldoon Abu-Hakmeh, P.S., Byeoung Jae Chun, Ji Il Choi, and Seung Soon Jang, *Effect of Uniaxial Deformation on Structure and Transport in Hydrated Nafion 117: Molecular Dynamics Simulation Study.* Materials Performance and Characterization, 2015. **4**: p. 131-147.

[19] Catalog, S.-A.; Available from: http://www.sigmaaldrich.com/chemistry.html.

[20] Berry, D.T.M.a.R.S., *Effect of potential energy topography on dynamics and phase behavior of clusters.* Molecular Physics, 1996. **88**: p. 709-726.

[21] Robert K. Z. Tan, A.S.P., and Stephen C. Harvey, *YUP: A Molecular Simulation Program for Coarse-Grained and Multiscaled Models.* Journal of Chemical Theory and Computation, 2005. **2**: p. 529-540.

[22] Marilisa Neri, C.A.M.C., Amos Maritan, and Paolo Carloni, *Coarse-Grained Model of Proteins Incorporating Atomistic Detail of the Active Site.* Physical Review Letters, 2005. **95**: p. 218102.

[23] Dumitru Pavel, R.S., *Molecular dynamics simulation of diffusion of O_2 and CO_2 in amorphous poly(ethylene terephthalate) and related aromatic polyesters.* Polymer, 2003. **44**: p. 6713-6724.

[24] C.W.T. Bulle-Lieuwma, W.J.H.v.G., J.K.J. van Duren, P. Jonkheijm, R.A.J. Janssen, J.W. Niemantsverdriet, *Characterization of polymer solar cells by TOF-SIMS depth profiling.* Applied Surface Science, 2003. **203-204**: p. 547-550.

[25] Naga Rajesh Tummala, S.M., Yao-Tsung Fu, Chad Risko, Jean-Luc Bredas, *Materials-Scale Implications of Solvent and Temperature on [6,6]-Phenyl-C61-butyric Acid Methyl Ester (PCBM): A Theoretical Perspective.* Advance Functional Materials, 2013. **23**: p. 5800-5813.

[26] Jillian A. Emerson, D.T.W.T., Jonathan R. Howse, Eric M. Furst, and Thomas H. Epps, III, *Determination of Solvent-Polymer and Polymer-Polymer Flory Huggins Interaction*

Parameters for Poly(3-hexylthiophene) via Solvent Vapor Swelling. Macromolecules, 2013. **46**: p. 6533-6540.

[27] Accelrys, I., *Cerius*^{2}. 2014, Accelrys, Inc.: San Diego, CA.

[28] Accelrys, I., *Materials Studio*. 2014, Accelrys, Inc.: San Diego, CA.

[29] Tina Duren, F.M., Gerard Ferey, Krista S. Walton, and Randall Q. Snurr, *Calculating Geometric Surface Areas as a Chrarcterization Tool for Metal-Organic Frameworks.* Journal of Physical Chemistry, 2007. **111**: p. 15350-15356.

[30] G. Yu, J.G., J. C. Hummelen, F. Wudl and A. J. Heeger, *Polymer Photovoltaic Cells: Enhanced Efficiencies via a Network of Internal Donor-Acceptor Heterojunctions.* Science, 1995. **270**: p. 1789-1791.